The effect of discharge chamber geometry on the ignition of low-pressure rf capacitive discharges

V. Lisovskiy
Laboratoire de Physique et Technologie des Plasmas, Ecole Polytechnique, Palaiseau 91128, France and Kharkov National University, Kharkov 61077, Ukraine

S. Martins, K. Landry, and D. Douai
Unaxis Displays Division France SAS, 5, Rue Leon Blum, Palaiseau 91120, France

J.-P. Booth
Laboratoire de Physique et Technologie des Plasmas, Ecole Polytechnique, Palaiseau 91128, France

V. Cassagne
Unaxis Displays Division France SAS, 5, Rue Leon Blum, Palaiseau 91120, France

V. Yegorenkov
Kharkov National University, Kharkov 61077, Ukraine

(Received 13 June 2005; accepted 5 July 2005; published online 2 September 2005)

This paper reports measured and calculated breakdown curves in several gases of rf capacitive discharges excited at 13.56 MHz in chambers of three different geometries: parallel plates surrounded by a dielectric cylinder ("symmetric parallel plate"), parallel plates surrounded by a grounded metallic cylinder ("asymmetric parallel plate"), and parallel plates inside a much larger grounded metallic chamber ("large chamber"). The breakdown curves for the symmetric chamber have a multivalued section at low pressure. For the asymmetric chamber the breakdown curves are shifted to lower pressures and rf voltages, but the multivalued feature is still present. At higher pressures the breakdown voltages are much lower than for the symmetric geometry. For the large chamber geometry the multivalued behavior is not observed. The breakdown curves were also calculated using a numerical model based on fluid equations, giving results that are in satisfactory agreement with the measurements. © *2005 American Institute of Physics*.
[DOI: 10.1063/1.2033748]

I. INTRODUCTION

Low-pressure rf capacitive discharges are widely used for etching and surface modification of various materials; for depositing oxides, nitrides, and other films, for cleaning deposition chambers, in plasma chemistry, and for medical tool sterilization. Breakdown curves, which describe the conditions under which rf discharges can occur, are a fundamental characteristic of these discharges. A brief review of rf discharge ignition has been published previously.[1–3] Lisovskiy and Yegorenkov[2] propose that several branches can be distinguished in the breakdown curves (emission-free, diffusion-drift, Paschen, and multipactor), according to the dominant generation and loss processes of the charged particles. In a later paper[3] the same authors give a detailed description of the correct method for measuring rf discharge breakdown curves and describe the necessary experimental setup. Breakdown curves can only be measured unambiguously when there is a uniform, parallel rf electric field across the chamber. This is achieved with planar, parallel electrodes surrounded by a closely fitting tube of a dielectric material. Objects such as electrostatic probes and substrate holders must be absent from the discharge chamber because they will seriously distort the vacuum rf field.

It has been shown that, for pressures below the minimum in the breakdown curve of parallel-plate rf discharges, one can observe a region of multivalued dependence of the rf breakdown voltage U_{rf} on the gas pressure p.[1–4] The reason for this phenomenon is the increased loss of the electrons to the electrodes due to the large amplitude of their oscillations in large rf electric fields at low gas pressure. However, Smith *et al.*[5] measured rf breakdown curves in a discharge chamber with a more complex geometry (with small-diameter electrodes placed inside a large chamber with grounded metallic walls) and found no multivalued feature. They observed U-shaped breakdown curves, similar to the dc Paschen breakdown curve observed for a discharge with a large distance between the electrodes. Rather than attempting to explain why they did not observe a multivalued section in their experiment, they chose to question the previous measurements.[1–4] The multivalued feature of the breakdown curves was also not observed in other experiments[6] carried out in a so-called "GEC reference cell."[7,8]

The objective of this paper, therefore, is to study how discharge chamber geometry affects the shape of breakdown curves for rf capacitive discharges. We have studied three different chamber geometries : (1) Parallel plates surrounded by a dielectric cylinder ("symmetric chamber"); (2) parallel plates surrounded by a grounded metallic cylinder ("asymmetric chamber"); and (3) parallel plates inside a much larger grounded metallic chamber ("large chamber"), similar to the GEC (Gaseous Electronics Conference) reference cell.[7,8] We demonstrate experimentally that breakdown

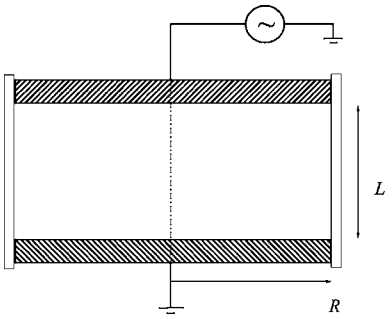

FIG. 1. Schematic of the symmetric rf discharge.

curves can only be correctly measured when the radial boundary of the parallel-plate electrodes is comprised of a dielectric tube (the symmetric chamber configuration). With this configuration our results are in good agreement with those of other authors in the region near to, and to the right of, the minimum of the diffusion-drift branch. However, when the distance between the electrodes is sufficiently large, the multivalued behavior is observed to the left of the minimum. When the dielectric tube is replaced with a grounded metallic wall (asymmetric chamber) the breakdown curve is shifted to lower pressures and rf voltages, but the multivalued feature is still present. At higher gas pressure breakdown occurs at much lower voltages than for the symmetric chamber. For chambers that consist of small (parallel) electrodes inside a large discharge chamber with grounded walls (the large chamber, comparable to the GEC reference cell) no multivalued section is observed.

A fluid simulation in two-dimensional cylindrical geometry was developed to explain these results, giving results in satisfactory agreement with the experimental observations for the three discharge chamber configurations under study.

II. EXPERIMENT

Experiments were performed in two different vacuum vessels and for three different configurations, which we shall denominate as (1) the symmetric chamber, (2) the asymmetric chamber, and (3) the large chamber.

The first vacuum vessel consists of a 315-mm-diam, 231-mm-high steel chamber, with a viewport to observe breakdown. Two parallel 143-mm-diam aluminum electrodes are installed in this vessel. The upper (powered) electrode is 10 mm thick, and on its upper side is separated from a grounded shield (20 mm thick) by a layer of dielectric material. The lower (grounded) electrode is 30 mm thick. The gas was input through small holes in the upper (powered) electrode, and evacuated via the external chamber. The gas pressure was monitored with capacitance manometers (10 and 1000 Torr, MKS Instruments). A constant gas flow of 5 sccm was set with a mass flow controller. The gas pressure was set by a feedback-controlled valve on the pumping outlet. An rf probe (Advanced Energy Z'SCAN) was used to measure the rf voltage amplitude U_{rf}, the rf current I_{rf}, the phase shift φ between the rf voltage and rf current, and the delivered power. It was situated as close as possible to the rf electrode. The rf power (13.56 MHz) was supplied by an rf

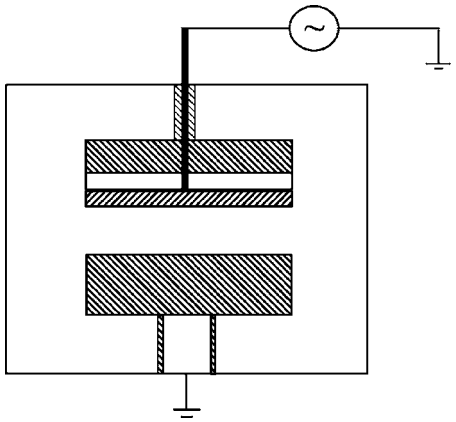

FIG. 2. Schematic of the large chamber configuration.

generator (RF Power Products Inc., RF5S) via an L-type matchbox (Huttinger Elektronik Gmbh PFM).

In the "symmetric chamber" configuration, the two electrodes were surrounded by a 145-mm internal diameter (i.d.) fused silica tube, so that the effective discharge volume resembles Fig. 1. In the "large chamber" configuration (Fig. 2) the same electrodes were used, but the fused silica tube was removed so that the electrodes were located within a metallic chamber with grounded walls. This discharge configuration is similar to that used by the authors of Ref. 5, allowing us to obtain similar results and to compare them to the symmetric chamber. Similar chamber configurations are widely used for studying the characteristics of the rf discharges (see, e.g., Ref. 9–19). Experiments in this vessel were performed in argon, nitrogen, hydrogen, and helium over the pressure range $p \approx 0.01$–10 Torr with an rf field frequency of $f = 13.56$ MHz. The breakdown curves were recorded for interelectrode gap values of $L = 11.9$ mm, $L = 20.4$ mm, and (in some experiments) $L = 27$ mm.

We performed some experiments in a second vacuum vessel comprised simply of planar parallel stainless-steel electrodes of 100 mm diam inside a fused silica tube. The electrodes completely filled the cross section of the discharge tube. The gas delivery and exhaust were accomplished through groups of small holes in one of the electrodes. In this case the interelectrode distance was 33 mm. In this "symmetric chamber" configuration, very similar results were obtained as for the first vacuum vessel in the symmetric configuration. This vacuum vessel was also used to achieve the third, "asymmetric chamber" configuration (Fig. 3). In this

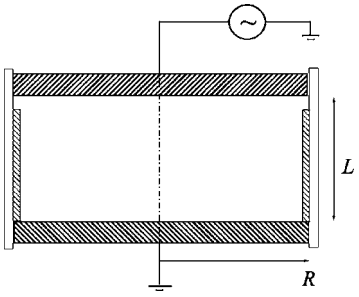

FIG. 3. Schematic of the asymmetric chamber, with foil on the radial walls.

case the inner surface of the 100-mm-diam discharge tube was covered with a grounded aluminum foil. A gap of 2 mm was left between the foil edge and the surface of the rf electrode. Similar chambers (from the viewpoint of the asymmetric distribution of the vacuum rf field) have also been widely used in other studies of rf discharges.[20–28]

We used the technique proposed by Levitskii[4] to record the rf discharge breakdown curves. In the vicinity of, and to the right of, the breakdown curve minimum, first the gas pressure was fixed and then the rf voltage increased slowly until breakdown occurred. At pressures below the breakdown minimum, the curve may have a multivalued dependence on the rf voltage. Therefore, in this region, the gas pressure was first decreased (to prevent breakdown), then the rf voltage was set to a given value, and then the gas pressure was slowly increased until discharge ignition occurred. When this occurs, the rf voltage is seen to drop abruptly, and a glow appears between the electrodes. The rf voltage was measured to an accuracy better than 1–2 V. The rate of the rf voltage increase before the breakdown was below 1 V/s, therefore the time lag for the onset of discharge ignition did not noticeably affect the recorded breakdown voltage values.

III. FLUID SIMULATION

Gas breakdown in rf electric fields occurs when the number of charged particles created in the discharge gap (either by ionization of gas molecules via electron impact or by secondary electron emission from the electrode surfaces and chamber walls) exceeds the electron losses to the walls due to diffusion and drift in the rf field (and also electron attachment, if the gas is electronegative). The breakdown process can be described by the fluid equations for electron density conservation in cylindrical geometry:

$$\frac{\partial n_e}{\partial t} = \nu_i n_e + D_e \frac{1}{r}\frac{\partial}{\partial r}\left(r\frac{\partial n_e}{\partial r}\right) + D_L \frac{\partial^2 n_e}{\partial z^2} - V_e \cdot \nabla n_e \cdot \cos(\omega t) = 0, \tag{1}$$

where n_e is the electron number density, t is time, V_e is the electron drift velocity, $\nu_i = \alpha V_e$ is the rate of ionization of gas molecules via electron impact, α is the first Townsend coefficient, D_L and D_e are the electron diffusion coefficients along and across the electric field respectively, r and z are the radial and axial coordinates, $\omega = 2\pi f$ is the electric field angular frequency, and f is the linear frequency of the rf generator. All calculations were performed for argon and for the chamber configurations described above.

In order to solve Eq. (1) it is necessary to know the electron transport coefficients, α, D_L, D_e and V_e, in the given gas. These coefficients were calculated over a broad range of E/p (the ratio of the electric field strength to the gas pressure) using the BOLSIG code (Kinema Research and Software, www.kinema.com). The results were then fitted to simple analytic formulas for convenience. Equation (1) was then solved using a commercial finite-element method solver FEMLAB (COMSOL, Inc., www.comsol.com). The rate of ionization of molecules via electron impact was assumed to be determined by the *effective* rf field and therefore invariant with rf phase:

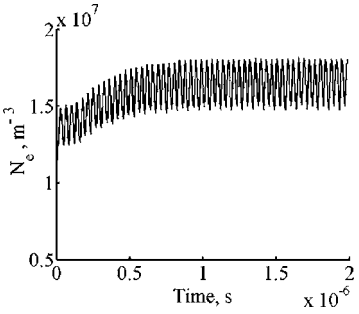

FIG. 4. Electron density as a function of time at the gap center of a symmetric rf discharge with an argon pressure of 0.15 Torr.

$$E_{\text{eff}} = \frac{E_{\text{rf}}}{\sqrt{2}} \frac{\nu_{en}}{\sqrt{\omega^2 + \nu_{en}^2}}, \tag{2}$$

where E_{rf} is the amplitude of the rf field and ν_{en} is the rate of electron-neutral collisions.

Consider first the discharge gap between parallel-plate electrodes. The lower electrode ($z=0$) is grounded and the upper one ($z=20.4$ mm) is set to an rf voltage $U = U_{\text{rf}} \cos(\omega t)$. The lateral (radial) walls of the discharge chamber are assumed to be of a dielectric material and are at floating potential. Secondary electron emission from the surface of the electrodes or the walls of the discharge tube was not included, i.e., the following boundary conditions for the electron concentration were used:

$$N_e(R,z) = 0, \quad n_e(r,0) = 0, \quad n_e(r,L) = 0, \tag{3}$$

where R is the tube radius and L is the interelectrode distance. The initial electron concentration at $t=0$ was set to $n_{e0} = 10^7$ m^{-3}. Such a low electron density does not distort the vacuum distribution of the rf electric field in the gap. The calculations were performed for the first 30 periods of the rf field; this was quite adequate in most cases to determine whether or not the average electron density increases (leading to breakdown) for given values of the argon pressure and rf voltage amplitude. With an argon pressure of $p \geqslant 10$ Torr, the calculations were performed for 60 periods of the rf field because, in this case, the electron density varies more slowly. The rf voltage amplitude, was varied to find the value, U_{rf0}, at which the electron density at the discharge center (averaged over the rf field period) remains unchanged after the first 10–15 periods. This value of the rf voltage amplitude was taken to be the breakdown rf voltage. An example is shown in Fig. 4, which shows the temporal dependence of the electron density at the discharge gap center. For rf voltage amplitudes below the breakdown value, the initial electron concentration decreases rapidly with time, demonstrating the excess of electron losses over generation, and the rf discharge does not ignite under these conditions. For voltage amplitudes above this critical value, the average electron density continually increases with time, indicating the onset of rf discharge ignition.

Similar initial and boundary conditions were also used for the other, more complicated designs presented in Figs. 2 and 3. That is, the amplitude of the rf potential at the powered electrode was set to U_{rf}, the dielectric surfaces (the tube

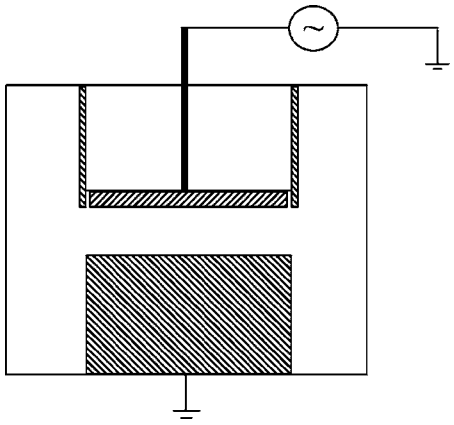

FIG. 5. Schematic of a chamber similar to the GEC reference cell.

walls in Fig. 1, the surface of the dielectric of the upper electrode in Fig. 2) acquired the floating potential, and all other surfaces (being grounded in the experimental devices) had zero potential. All of the geometrical details of the actual discharge chambers were reproduced in the simulations. We did not make measurements in an actual GEC reference cell because no such chamber was available. However, we did calculate the rf breakdown curve for such a chamber filled with argon gas. More precisely the calculations were performed for a chamber design similar to Fig. 2, but somewhat changed to be similar to a GEC reference cell (see Fig. 5).[7,8] In this case, we assumed the rf voltage to be applied only to the plane surface of the rf electrode, whereas the edge of the rf electrode was surrounded with a grounded screen (in agreement with the design of the GEC reference cell). The authors of Refs. 29 and 30 also used chambers similar to the GEC reference cell.

IV. RESULTS

Let us consider how the discharge chamber configuration affects the rf capacitive discharge breakdown curves. Figure 6 shows our measured rf breakdown curves in argon with an interelectrode distance of $L=20.4$ mm for the symmetric and large chamber configurations. For the symmetric configuration the drift-diffusion branch possesses a multivalued section to the left of the breakdown minimum which, at $U_{\mathrm{rf}} > 200$ V, transforms into the Paschen branch. Also shown are the results of Sato and Shoji,[31] who measured the breakdown curve in argon in the vicinity and to the right of the minimum for $L=20$ mm, in good agreement with our results.

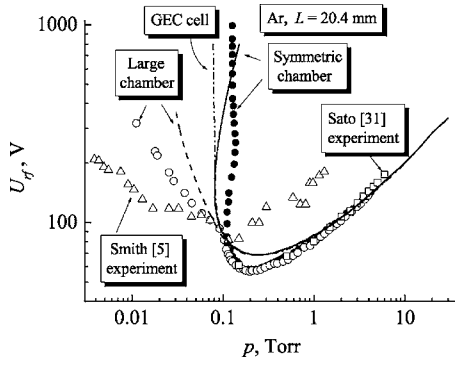

FIG. 6. Breakdown curves of an rf discharge in argon at $L=20.4$ mm: Full circles and empty circles are our measured data for the symmetric discharge and for the large chamber, respectively; empty triangles depict the experimental data from Ref. 5 (electrodes inside a large chamber, $L=20$ mm); empty squares depict the experimental data from Ref. 31 (parallel-plate rf discharge, $L=20$ mm); solid line, dashed line, and dashed–dotted line depict our calculated data for the parallel-plate rf discharge, electrodes in a large chamber, and a GEC cell, respectively.

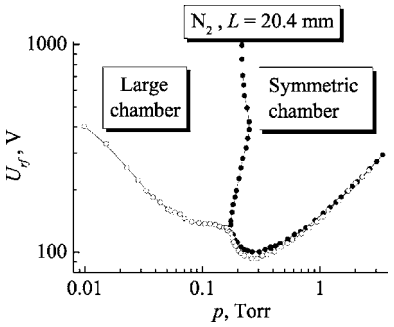

FIG. 7. Breakdown curves of an rf discharge in nitrogen at $L=20.4$ mm: Full circles and empty circles are for our measured data for the symmetric discharge and for planar electrodes in a large chamber, respectively.

Figure 6 also shows the results for the large chamber configuration (Fig. 2). These are very similar to the symmetric chamber at pressures above 1 Torr, but for lower pressures the breakdown curve shifts to lower rf voltages. At the minimum it lies 2–3 V below the curve of the symmetric chamber. Thereafter, this curve appears to approach the same turning point as for the symmetric case, but then deviates toward lower pressure values, and possesses no multivalued section at all.

The breakdown curve we observed for the large chamber configuration agrees qualitatively with the results of Smith *et al.*[5] Their results, although showing a large spread, consist of two branches joined by a dogleg feature at $p \approx 0.08$ Torr. In contrast, above 0.1 mTorr their values of the breakdown rf voltage are higher than ours (and those of Sato and Shoji). The uncertainty in measuring the rf voltage values in Smith *et al.* was probably associated with the use of an rf probe *inside* the match box[32] to measure the rf voltage. They give no indication how far the measurement point was from the rf electrode, and did not discuss the correspondence between

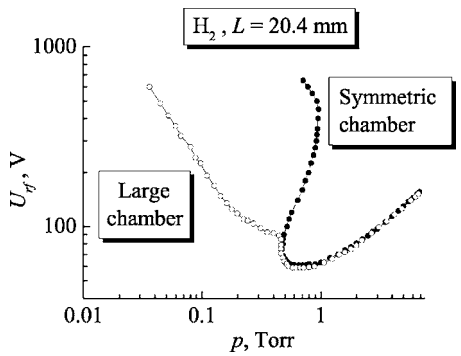

FIG. 8. Breakdown curves of the rf discharge in hydrogen at $L=20.4$ mm: Full circles and empty circles are for our measured data for the symmetric discharge and for planar electrodes in a large chamber, respectively.

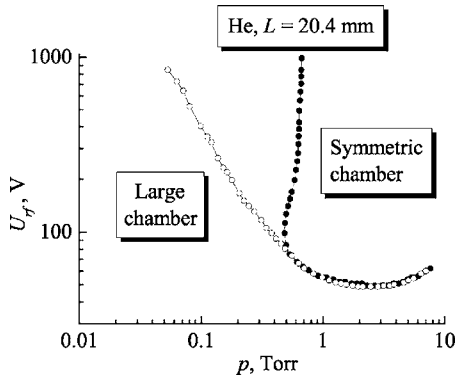

FIG. 9. Breakdown curves of the rf discharge in helium at $L=20.4$ mm: Full circles and empty circles are for our measured data for the parallel-plate discharge and for planar electrodes in a large chamber, respectively.

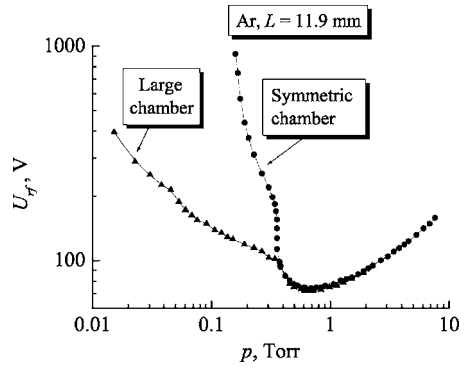

FIG. 10. Breakdown curves of the rf discharge in argon at $L=11.9$ mm: Full circles depict the breakdown curve for the symmetric discharge; full triangles depict the breakdown curve for the planar electrodes in a large chamber, respectively.

this measured voltage and the actual rf voltage at the electrode.

The results of our calculations are also shown in Fig. 6. In the pressure range above 1 Torr they are close to the experimental data, and to those of Sato and Shoji. At lower pressure, the calculated curves lie somewhat above the measured ones. The calculated curve for the symmetric configuration lies very close (approximately 2 V above) to that for the large chamber (in agreement with the results of our measurements). On further decreasing the pressure, the calculated curve for the symmetric configuration passes through a turning point and deviates back towards higher pressure, i.e., we observe a multivalued section. The calculated curve for the large chamber is simply U-shaped and does not contain a multivalued section. In the calculations we did not include electron-induced secondary electron emission from any surfaces. It has been shown that the presence of secondary electron emission from the electrode surfaces shifts the breakdown curve to lower voltages.[1,33,34] Smith *et al.*[5] also drew similar conclusions on the role of secondary emission. However, our aluminum electrodes were undoubtedly covered with an oxide film with an unknown secondary electron emission coefficient, δ (for Al_2O_3 the maximum reported values of the coefficient δ vary from 1.5 to 4.8[35]). Furthermore, the emission properties of the stainless-steel walls of the large discharge chamber are unknown. Therefore, we preferred to neglect secondary emission, and the calculated breakdown curves should be regarded as the maximum values of the rf breakdown voltage.

The breakdown curves for nitrogen and hydrogen are shown in Figs. 7 and 8 for the symmetric and large chamber configurations. The breakdown curves for the symmetric chamber in nitrogen, hydrogen, and helium again possess a multivalued section. The curves for the large chamber configuration are very similar (but slightly lower) in the drift-diffusion section, but on approaching the turning point they deviate abruptly towards lower pressure. For helium (Fig. 9) the breakdown curve for the large chamber is U-shaped.

The breakdown curve for argon with a smaller distance between the electrodes ($L=11.9$ mm, Fig. 10) has a diffusion-drift branch, and for low pressures and rf voltages above 180 V we also observe the Paschen branch. The breakdown curve for the large chamber (with $L=11.9$ mm) is similar to the case of $L=20.4$ mm.

For nitrogen (Fig. 11) the breakdown curve for the symmetric configuration shows a diffusion-drift branch, a Paschen branch (for $U_{\mathrm{rf}} \approx 400$–$800$ V and $p<1$ Torr), and transits to a multipactor branch at pressures below 0.4 Torr. For the large chamber, the breakdown curve approaches the turning point of the diffusion-drift branch before deviating abruptly to lower rf voltages, giving a second minimum. To summarize, at pressures below the diffusion-drift branch, the breakdown curves are qualitatively different for the symmetric and large chambers for all of the gases studied here.

Now let us consider what causes the multivalued section to appear in the breakdown curve of the symmetric chamber. First, consider a point on the diffusion-drift branch to the right of the breakdown curve minimum. The rf discharge can be ignited when the electrons acquire, in the rf electric field, an energy exceeding the ionization potential of the gas molecules. The number of electrons generated by ionization must exceed the number of electrons lost to the electrodes and walls of the discharge chamber due to both diffusion and the oscillating motion (drift) in the rf field. Under sufficiently high gas pressure, the amplitude of the electron displacement in the rf field $A=eE_{\mathrm{rf}}/m\nu_{en}\omega$ (where e and m are the electron

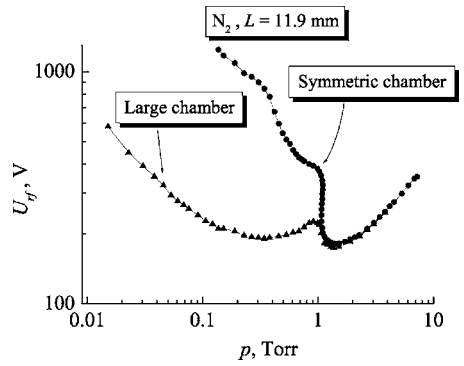

FIG. 11. Breakdown curves of the rf discharge in nitrogen at $L=11.9$ mm: Full circles depict the breakdown curve for the symmetric discharge; full triangles depict the breakdown curve for the planar electrodes in a large chamber, respectively.

charge and mass, respectively) is small compared with the interelectrode distance L, and the oscillating motion has little effect on the electron loss.

As the gas pressure is decreased, the rate of electron collisions with gas molecules decreases, so that their mean free path increases, and they gain more energy from the rf field between inelastic collisions, leading to more ionization. Therefore, rf breakdown can occur at lower rf voltages. However, as the gas pressure decreases further, the amplitude of the electron displacement A in the rf field increases and becomes a significant cause of electron loss. The loss due to diffusion also increases. These increasing losses must be compensated by more ionization. Therefore, the rf breakdown voltage approaches a minimum and then starts to increase. When the amplitude of the electron displacement amplitude becomes equal to one-half of the interelectrode distance $A=L/2$, the electron losses due to the oscillations in the rf field become very large (indeed, within the approximations of the fluid model they become infinite), and the breakdown curve passes through a turning point with the coordinates $p=p_t$ and $U_{\mathrm{rf}}=U_t$.

Let us now fix the gas pressure $p=p_t$ and apply an rf voltage slightly exceeding U_t. Under these conditions the amplitude of the electron displacement in the rf field exceeds one-half of the interelectrode distance, and the electrons are lost to the electrodes before they can have a sufficient number of ionizing collisions with gas molecules. Any further increase in the rf voltage will increase the losses more than the ionization, and cannot cause breakdown (until the voltage is high enough to pass into a resonant multipactor regime). Breakdown can only occur if the gas pressure is increased. Therefore, after running through the turning point the breakdown curve deviates towards higher gas pressure, and we observe a multivalued section of the rf breakdown curve. Thus, when the electrodes occupy the total cross section of the discharge tube and the discharge can ignite only within the gap between the planar electrodes, the distance between those electrodes determines the shape of the breakdown curve.

Now consider the case of planar electrodes installed inside a large chamber. At high gas pressure, the breakdown occurs between the electrodes, giving similar results to the symmetric chamber (the breakdown may tend to occur near the edges of the planar electrodes where the rf electric field is higher, giving slightly lower breakdown voltages). Rf breakdown will occur along any electric field line for which the ionization rate exceeds the losses. At high pressure this condition is satisfied first for electric field lines that directly cross the electrode gap. However, as the pressure is lowered, the amplitude of the displacement approaches one-half of the interelectrode distance and breakdown within the gap becomes impossible. Nevertheless, breakdown can now begin to occur via longer paths, for example, between the edge of the rf electrode and the external surface of the grounded electrode. Along these longer paths the electric field is lower (giving less ionization), but the distance is longer (increasing ionization and reducing losses). As is well known from measurements in symmetric chambers,[1–4,33] increasing the electrode spacing shifts the drift-diffusion branch to lower pressure. As the pressure decreases further, the discharge may ignite between the rf electrode and the grounded wall of the chamber and so forth. Thus with planar electrodes inside a large chamber the multivalued section of the breakdown curve is not observed, because for any pressure below the turning point $p=p_t$, an rf electric field line may be found (outside the gap between the planar electrodes), where with a sufficient rf voltage across the electrodes the electron losses are compensated by ionizing collisions, and the discharge can be ignited. This is the reason Smith *et al.* did not observe a multivalued section of the rf breakdown curve in their chamber.

Further understanding of this process can be obtained from the fluid simulations. Figure 12 shows the simulated electron concentration profiles during breakdown in the large chamber in low-pressure Ar. It is clear that the discharge ignites outside the gap between planar electrodes. At 0.01 Torr the discharge ignites close to the wall of the discharge chamber. On increasing the pressure, the discharge ignition region moves towards the electrodes. At ≈ 0.1 Torr the breakdown occurs around the electrode edges. At higher pressure, breakdown occurs within the interelectrode gap. These results are in good agreement with the observations of Githens[36] who measured rf discharge breakdown curves in the chambers of different design and presented clear photographs of the steady-state discharge for the case of small planar electrodes inside a large chamber.

We also performed the calculations for the chamber shown in Fig. 5, which is similar to the widely used GEC reference cell. These calculated breakdown curves are also presented in Fig. 6. It is clear that these calculated breakdown curves are U-shaped and do not have a multivalued section, in agreement with experimental observations in a GEC reference cell.[6]

Now let us consider the rf breakdown in the asymmetric chamber shown in Fig. 3. Figures 13 and 14 show the breakdown curves in argon and nitrogen, respectively, for both the symmetric and asymmetric configurations (i.e., with the inner surface of the fused silica tube almost completely covered with grounded aluminum foil). The breakdown curve for the symmetric configuration shows a diffusion-drift branch with a clearly expressed multivalued section. The breakdown curve for the asymmetric configuration also has a multivalued section, but the turning point is shifted to lower pressure and rf voltages. The minimum breakdown voltages are somewhat lower than for the symmetric case. Near the minimum, and to the right of it, the breakdown curves for both configurations coincide over a certain range of pressure. Over this range the breakdown occurs in the central region of the gap, so that the interelectrode spacing plays the determining role. On increasing the gas pressure further, the breakdown voltage for the asymmetric case is lower than for the symmetric case, and the spacing between the curves increases with pressure. For the experiments with a smaller diameter (100 mm) tube and larger interelectrode distance $L=33$ mm [Fig. 14(c)] the curves are already separate at their minima. In this chamber, the rf field nonuniformity, due to the presence of the foil on the tube wall, plays a substantial role over the whole range of gas pressure studied.

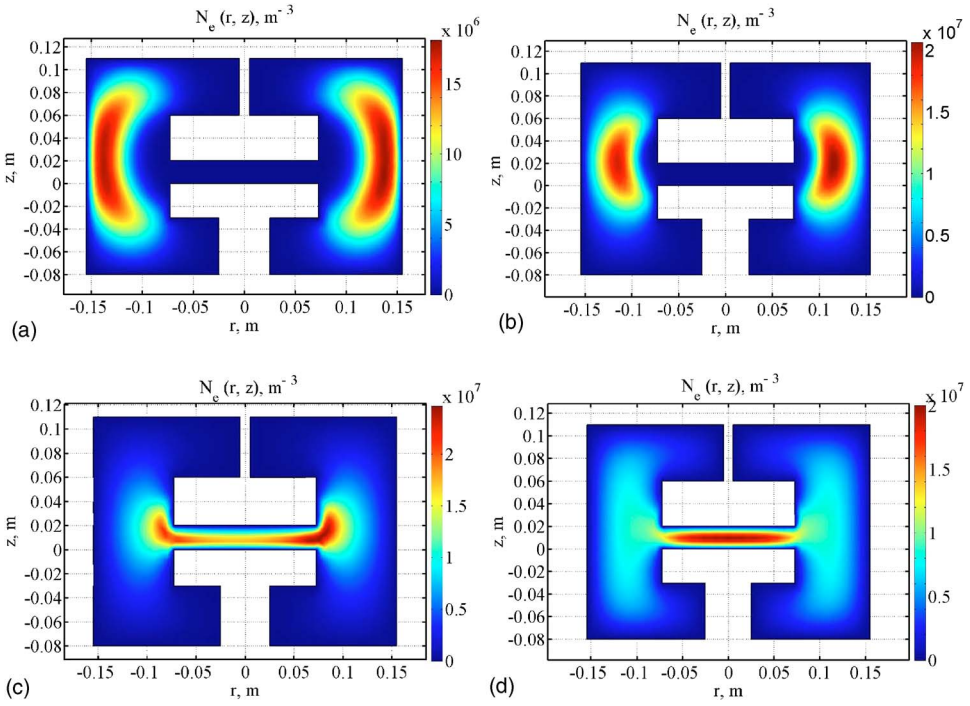

FIG. 12. (Color online) Electron density profiles in a large chamber with inner planar electrodes under conditions corresponding to discharge ignition:
(a) p=0.0275 Torr and U_{rf}=620 V,
(b) p=0.04 Torr and U_{rf}=218 V,
(c) p=0.1 Torr and U_{rf}=83 V,
(d) p=1 Torr and U_{rf}=87 V.

The asymmetric chamber has specific characteristics. Obviously, near the chamber axis the rf electric field is uniform, and the length of the electric field lines is equal to the interelectrode distance L. However, toward the edge of the chamber the electric field lines are distorted. There now exist field lines (specifically, from the corner of the grounded electrode/foil interface to the rf electrode), which are longer than L, and at low pressure, breakdown occurs here, at slightly smaller voltages than are observed for the symmetric chamber. Therefore, the breakdown curve in such nonuniform fields is shifted to lower pressures and rf voltages.

However, at pressures above the breakdown minimum, breakdown occurs at lower voltages for smaller discharge gaps. Therefore, the higher the pressure, the closer the breakdown region is to the edge of the rf electrode, where there are short field lines to the aluminum foil. As the rf field strength is much larger between the rf electrode and the foil, much lower rf voltages are required to ignite the discharge than for the symmetric configuration. Thus the behavior of the right-hand branch of the breakdown curve is due to the field nonuniformity caused by the grounded foil fixed to the wall of the discharge tube.

The calculated breakdown curves in argon for the symmetric and asymmetric chambers (Fig. 13) are in reasonable agreement with the observations. The presence of the multivalued section at low pressure and the divergence of the

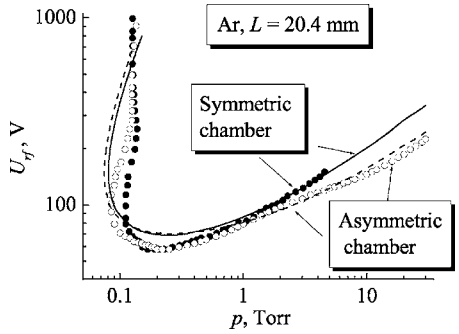

FIG. 13. Breakdown curves of an rf discharge in argon at L=20.4 mm: Full circles and empty circles depict our measurements for the symmetric discharge and for a discharge with foil on the tube wall, respectively; the solid line and dashed lines depict our calculated data for the symmetric rf discharge and for the asymmetric chamber, respectively.

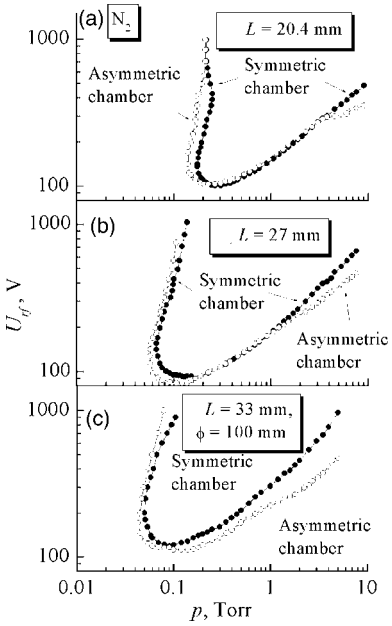

FIG. 14. Breakdown curves of an rf discharge in nitrogen (full circles and empty circles depict our measured data for the symmetric discharge and for the discharge with a foil on the tube wall, respectively) with the interelectrode distances: (a) L=20.4 mm; (b) L=27 mm (electrode diameter equals 143 mm); (c) L=33 mm (electrode diameter is 100 mm).

curves at higher pressure are clearly reproduced by the model.

V. CONCLUSIONS

Correct (Levitskii-type) measurements of the breakdown curves of rf discharges of different design give the following results. In a truly symmetric rf discharge, with the electrodes limited by a dielectric tube, the breakdown curve in the low-pressure range may possess a multivalued section. If the dielectric tube is replaced with a metallic grounded wall, the breakdown curve shifts to lower pressure and rf voltage values, but the multivalued section is still present. At higher gas pressures, the breakdown curve in this case runs much lower than for the parallel-plate rf discharge, and breakdown occurs between the planar surface of the rf electrode and the foil. When the small planar electrodes are located inside a large discharge chamber with grounded walls, as well as in the case of a GEC cell, the multivalued section is absent from the breakdown curves. The results of our fluid simulation are in satisfactory agreement with our measured data.

ACKNOWLEDGMENT

The authors express their gratitude to the Unaxis France–Displays Division, Palaiseau, France for their financial support and for the equipment used in this study.

[1] V. A. Lisovsky and V. D. Yegorenkov, J. Phys. D **27**, 2340 (1994).
[2] V. A. Lisovskiy and V. D. Yegorenkov, J. Phys. D **31**, 3349 (1998).
[3] V. A. Lisovskiy and V. D. Yegorenkov, J. Phys. D **32**, 2645 (1999).
[4] S. M. Levitskii, Sov. Phys. Tech. Phys. **2**, 887 (1957).
[5] H. B. Smith, C. Charles, R. W. Boswell, Phys. Plasmas **10**, 875 (2003).
[6] P. R. J. Barroy (private communication), 2003.
[7] J. K. Olthoff and K. E. Greenberg, J. Res. Natl. Inst. Stand. Technol. **100**, 327 (1995).
[8] M. A. Sobolewski, IEEE Trans. Plasma Sci. **23**, 1006 (1995).
[9] C. A. Anderson and W. G. Graham, Plasma Sources Sci. Technol. **4**, 561 (1995).
[10] V. Schulz-von der Gathen and H. F. Dobele, Plasma Chem. Plasma Process. **16**, 461 (1996).
[11] S. F. Adams and T. A. Miller, Plasma Sources Sci. Technol. **9**, 248 (2000).
[12] T. Gans, C. C. Lin, V. Schulz-von der Gathen, and H. F. Dobele, J. Phys. D **34**, L39 (2001).
[13] T. Gans, V. Schulz-von der Gathen, and H. F. Dobele, Plasma Sources Sci. Technol. **10**, 17 (2001).
[14] T. Gans, C. C. Lin, V. Schulz-von der Gathen, and H. F. Dobele, Phys. Rev. A **67**, 012707 (2003).
[15] T. Makabe, F. Tochikubo, and M. Nishimura, Phys. Rev. A **42**, 3674 (1990).
[16] F. Tochikubo, A. Suzuki, S. Kakuta, Y. Terazono, and T. Makabe, J. Appl. Phys. **68**, 5532 (1990).
[17] S. Kakuta, T. Makabe, and F. Tochikubo, J. Appl. Phys. **74**, 4907 (1993).
[18] H. Kawasaki, H. Ohkura, T. Fukuzawa, M. Shiratani, Y. Watanabe, Y. Yamamoto, S. Suganuma, M. Hori, and T. Goto, Jpn. J. Appl. Phys., Part 1 **36**, 4985 (1997).
[19] N. Spiliopoulos, D. Mataras, and D. Rapakoulias, Jpn. J. Appl. Phys., Part 1 **36**, 4717 (1997).
[20] P. Kae-Nune, J. Perrin, J. Guillon, and J. Jolly, Plasma Sources Sci. Technol. **4**, 250 (1995).
[21] O. Leroy, P. Stratil, J. Perrin, J. Jolly, and Ph. Belenguer, J. Phys. D **28**, 500 (1995).
[22] P. Kae-Nune, J. Perrin, J. Jolly, and J. Guillon, Surf. Sci. **360**, L495 (1996).
[23] G. J. Nienhuis, W. J. Goedheer, E. A. G. Hamers, W. G. J. H. M. van Sark, and J. Bezemer, J. Appl. Phys. **82**, 2060 (1997).
[24] O. Leroy, G. Gousset, L. L. Alves, J. Perrin, and J. Jolly, Plasma Sources Sci. Technol. **7**, 348 (1998).
[25] J. Perrin, M. Shiratani, P. Kae-Nune, H. Videlot, J. Jolly, and J. Guillon, J. Vac. Sci. Technol. A **16**, 278 (1998).
[26] M. Hertl and J. Jolly, J. Phys. D **33**, 381 (2000).
[27] N. Chaabane, A. V. Kharchenko, H. Vach, and P. Roca i Cabarrocas, New J. Phys. **5**, 37.1 (2003).
[28] A. V. Kharchenko, V. Suendo, and P. Roca i Cabarrocas, Thin Solid Films **427**, 236 (2003).
[29] L. Sansonnens, A. A. Howling, C. Hollenstein, J. L. Dorier, and U. Kroll, J. Phys. D **27**, 1406 (1994).
[30] Y. Watanabe, M. Shiratani, T. Fukuzawa, H. Kawasaki, Y. Ueda, S. Singh, and H. Ohkura, J. Vac. Sci. Technol. A **14**, 995 (1996).
[31] M. Sato and M. Shoji, Jpn. J. Appl. Phys., Part 1 **36**, 5729 (1997).
[32] H. B. Smith, C. Charles, R. W. Boswell, and H. Kuwahara, JSME Int. J., Ser. B **41**, 424 (1998).
[33] V. A. Lisovskiy, N. Yu. Kropotov, and V. I. Farenik, Tech. Phys. Lett. **22**, 1029 (1996).
[34] V. A. Lisovskiy and J.-P. Booth, Physical Surface Engineering **1**, 34 (2003).
[35] S. C. Brown, *Basic Data of Plasma Physics* (Wiley, New York, 1959).
[36] S. Githens, Phys. Rev. **57**, 822 (1940).